

Some effects of large blade deflections on aeroelastic stability

B.S. Kallesøe * and M.H. Hansen †

This paper concerns the effect of steady state deflection of a wind turbine blade on its aeroelastic stability. Modern wind turbines have long slender blades where the deflection can be considerable. Today, most aeroelastic stability tools do not take finite blade deflection into account when computing the stability of the turbine. In this study an aeroelastic model of a turbine blade, which include blade deflections, is developed and used for analyzing the effect of steady state blade deflections on the aeroelastic stability. It is found that the flutter speed for the RWT 63 m blade decrease when the steady state blade deflection is included in the analysis.

Nomenclature

$\bar{\mathbf{M}}$	Mass matrix for nonlinear partial differential equations of motion
$\bar{\mathbf{F}}$	Nonlinear response function for partial differential equations of motion
$\bar{\mathbf{f}}$	External forces for nonlinear partial differential equations of motion
$\bar{\mathbf{u}} = [u, v, \theta]^T$	Vector holding the nonlinear continues blade edgewise, flapwise and torsional elastic deflections
β	Blade pitch, rigid body rotation of the whole blade
ϕ	Rotor azimuth angle
\mathbf{f}_{aero}	Vector with the aerodynamic lift and drag forces
M_{aero}	Aerodynamic twisting moment (nose up)
t	Time
s	Radial position measured along elastic axis from rotor center
$\mathbf{U}_{3/4}$	Apparent wind velocity in the 3/4 chord point
\mathbf{U}	Apparent wind velocity neglecting pitch rate of the blade-section
\mathbf{T}_c	Transformation from a curved frame following the chord to a frame following the root of the blade
\mathbf{T}_β	Transformation from a frame following the root of the blade to a frame following the blade parallel to the rotor plane
U_t	Wind speed in the rotor plane
U_n	Free wind speed normal to the rotor plane
w	Radius from rotor center
a	Non-dimensional induced velocity normal to the rotor plane
a'	Non-dimensional induced velocity in the rotor plane
$\dot{\mathbf{r}}_{3/4}$	Position vector of 3/4 chord point
$\alpha_{3/4}$	Angle of attack at the 3/4 chord point
α	Angle of attack neglecting pitch rate of the blade-section
l_{pi}	Distance from pitch axis to elastic axis along the chord
l_{ac}	Distance from elastic axis to aerodynamic center along the chord
$[C_L, C_D, C_M]$	Aerodynamic lift, drag and moment coefficients
\mathbf{F}_{st}	Discretised steady state nonlinear equations of motion
\mathbf{f}	Discretised steady state aerodynamic forces
\mathbf{u}_0	Discretised steady state deflections
$\bar{\mathbf{A}}, \bar{\mathbf{B}}_{ss}, \bar{\mathbf{B}}_s, \bar{\mathbf{B}}$	Matrices for linear partial differential equations of motion

*Research Scientist, Wind Energy Department, Risø-DTU, Technical University of Denmark, DK-4000 Roskilde, Denmark.

†Senior Scientist, Wind Energy Department, Risø-DTU, Technical University of Denmark, DK-4000 Roskilde, Denmark.

$\bar{\mathbf{u}}$	Continues linear deflections, velocities and aerodynamic states
\mathbf{A}, \mathbf{B}	Matrices for discretised linear ordinary differential equations of motion
\mathbf{u}	Discritised linear deflections, velocities and aerodynamic states

I. Introduction

This paper concerns the effect of steady state blade deflections of wind turbine blade on its stability, especially with regards to the flutter limit. Modern wind turbines has long slender blades where the deflection can be considerable both under normal operation around rated power and especially in some fault situations, such as over-speed. The coupling of bending and torsion due to large flapwise blade deflection is assumed to have some effects on the flutter limits, as discussed in Hansen.¹ In this paper the effect of steady state blade deflection on the flutter speed is analyzed by an over-speed situations. The analysis is based on the structural blade model from Kallesøe,^{2,3} which includes effect of finite blade deflections. First the structural model is combined with an steady state aerodynamic model and discretized by an finite difference schema. The resulting nonlinear aeroelastic model is used to compute steady state deflection of a blade from the 5 MW Reference Wind Turbine (RWT) by NREL.⁴ Next the structural model is combined with an unsteady aerodynamic model⁵ and linearized about both the steady state deflected blade and an undeflected blade. A finite difference discretization of this linear unsteady aeroelastic model forms a differential eigenvalue problem, which is solved to give damping, frequencies and shapes of the aeroelastic modes of motion of the steady state deflected blade and the straight blade. The results from the deflected blade shows good qualitative agreement with nonlinear aeroelastic simulations with the HAWC2^{a6,7} code.

II. The Model

This section deals with the description of the aeroelastic models. First, a steady state aeroelastic model is set-up by combining the nonlinear structural model with a stationary aerodynamic model. Next, a linear unsteady aeroelastic model is set-up. The linear model is used in two configurations, one linearized about the steady state deflected blade, and one linearized about an undeflected blade. In the next section, the nonlinear steady state model is used to compute the steady state blade deflections at different wind speeds, rotor speeds, and the linear unsteady model is used to compute damping, frequencies and shapes of aeroelastic modes of motion.

A. Structural Blade Model

The structural blade model is based on the model described in Kallesøe^{2,3} using second order Bernoulli-Euler beam theory resulting in a nonlinear partial integro-differential equations of motion:

$$\bar{\mathbf{M}}\ddot{\bar{\mathbf{u}}} + \bar{\mathbf{F}}(\dot{\bar{\mathbf{u}}}, \bar{\mathbf{u}}', \bar{\mathbf{u}}, \ddot{\beta}, \dot{\beta}, \beta, \ddot{\phi}, \dot{\phi}, \phi) = \bar{\mathbf{f}}(f_{aero}, M_{aero}, u', v') \quad (1)$$

where $\bar{\mathbf{u}} = [u(t, s), v(t, s), \theta(t, s)]$ is the state vector holding edgewise, flapwise and torsional elastic deformations, s is the radial position along the blades elastic axis, t is the time, $\beta = \beta(t)$ is the controllable pitch of the blade, $\phi = \phi(t)$ is the azimuth angle of the rotor and the right hand side holds the effect of the aerodynamic forces (f_{aero}, M_{aero}) on the blade. Longitudinal forces on or in the blade, e.g. the centrifugal force, leads to integral terms in the equation. These equations of motion includes the effect of large blade deformation, gravity, pitch action and rotor speed variations. In this work the pitch is set to zero and kept constant ($\beta = 0, \dot{\beta} = 0$) and the rotor speed is constant within each test case ($\dot{\phi} = \text{cons.}, \ddot{\phi} = 0$).

B. Aerodynamic Models

The aerodynamic forces on the blade are described by two aerodynamic models, one for steady state conditions and one for unsteady conditions. These aerodynamic models are coupled to the structural model through the apparent wind speed and angle of attack, both depending on the deformation and the motion

^aAeroelastic code intended for calculating wind turbine response in time domain and has a structural formulation based on multi-body dynamics. The aerodynamic part of the code is based on the blade element momentum theory, but extended from the classic approach to handle dynamic inflow, dynamic stall, skew inflow, shear effects on the induction and effects from large deflections. It has been developed at the aeroelastic design research programme at Risø-DTU.

of the blade. The structural model is dependent on the aerodynamic model through the aerodynamic forces acting on the blade.

1. Apparent wind Velocity

The apparent wind velocity at the three-quarter chord point is used in the aerodynamic model. Formulated in the coordinates along the chord (towards the leading edge), normal to the chord (towards the suction side) and along the blade (towards the tip) the apparent wind velocity at the three-quarter chord point is:

$$\mathbf{U}_{3/4} = \mathbf{T}_c \mathbf{T}_\beta \left(\begin{bmatrix} -(U_t + w\dot{\phi})(1 + a') \\ U_n(1 - a) \\ 0 \end{bmatrix} - \dot{\mathbf{r}}_{3/4} \right) \quad (2)$$

where \mathbf{T}_c and \mathbf{T}_β are the transformations from a curved frame following the chord to a frame following the root of the blade, and from a frame following the root of the blade to a frame following the blade in the rotor plane, respectively. Both transformations are described in Kallesøe.^{2,3} The relative wind in the rotor plane caused by rotation of the rotor is given by $w\dot{\phi}$, where $w = w(s)$ is the radial distance from the rotor center and $a' = a'(s, t)$ is the non-dimensional induced velocity in the rotor plane. The free inflow is given by $U_n = U_n(s, t)$ and $a = a(s, t)$ is the non-dimensional induced velocity normal to the rotor plane. The induced velocities can be determined by e.g. beam element momentum theory.⁸ The induced velocities and tip loss are neglected in this work. Since this is a qualitative study on the effect of including large blade deflections in the aeroelastic analysis, the quantitative differences by neglecting induced velocities and tip loss are acceptable. The position vector $\mathbf{r}_{3/4} = \mathbf{T}_\beta^T \left(\begin{bmatrix} u + l_{pi} & v & w \end{bmatrix}^T + \mathbf{T}_c^T \begin{bmatrix} l_{3/4} & 0 & 0 \end{bmatrix}^T \right)$ defines the position of the three quarter chord point of the blade. The apparent wind velocity without pitch rate of the blade section $\mathbf{U} = \mathbf{U}_{3/4}|_{\dot{\beta}=\dot{\beta}=\dot{\theta}=\dot{\theta}=0}$ is also used in the aerodynamic model.

2. Angle of Attack

The angle of attack is the angle between the direction of the apparent wind and the chord, which is given by^b

$$\alpha = -\arctan\left(\frac{\mathbf{U}[2]}{\mathbf{U}[1]}\right) \text{ and } \alpha_{3/4} = -\arctan\left(\frac{\mathbf{U}_{3/4}[2]}{\mathbf{U}_{3/4}[1]}\right) \quad (3)$$

without and with pitch rate of the blade section, respectively.

3. Aerodynamic Forces

The aerodynamic forces on the blade are given by

$$\mathbf{f}_{aero} = \mathbf{T}_c^T \frac{1}{2} \rho c U \begin{bmatrix} C_D \mathbf{U}[1] + C_L \mathbf{U}[2] \\ C_D \mathbf{U}[2] - C_L \mathbf{U}[1] \\ 0 \end{bmatrix} \quad (4a)$$

$$M_{aero} = \frac{1}{2} \rho c^2 U^2 C_M + (\mathbf{f}_{aero}[2] l_{ac} \cos(\theta + \bar{\theta}) - \mathbf{f}_{aero}[1] l_{ac} \sin(\theta + \bar{\theta})) \quad (4b)$$

where $U = \sqrt{\mathbf{U}[1]^2 + \mathbf{U}[2]^2}$ is the apparent wind speed, ρ is the air density, l_{ac} is the distance from elastic axis to aerodynamic center along the chord and c is the local chord. The lift, drag and moment coefficients (C_L, C_D, C_M) are given by airfoil data for steady state conditions or by the unsteady aerodynamic model by Hansen et al.⁵ (described shortly in Kallesøe^{3,9}) for unsteady conditions.

C. Steady State Aeroelastic Model

Steady state conditions are defined as: Uniform inflow ($\dot{U}_n = 0$ and $U_t = 0$) and all time derivatives in the structural equations of motion (1) are zero $\ddot{u} = \ddot{v} = \ddot{\theta} = \dot{u} = \dot{v} = \dot{\theta} = 0$.

^bThe notation $\mathbf{U}[i]$ denotes the i 'th component of the vector \mathbf{U} .

1. Finite Difference Discretization of the Steady State Model

The spatial derivatives of the partial differential equations of motion (1) are approximated by a second order finite difference scheme with step size h and N computation points. The derivatives of parameters (such as mass, stiffness, etc.) are approximated by the same finite difference scheme. Integral terms are approximated by sums using the trapezoid rule. The boundary conditions for the finite difference formulation is derived by inserting the finite difference approximations into the boundary conditions expressions from Kallesøe.^{2,3} It is assuming that the offset of center of gravity is small at the blade tip, making the boundary condition independent of rotor position and speed.

2. Steady State Model

The discretized version of the steady state partial differential equations of motion (1) is implemented on the N discretization points leading to a nonlinear algebraic equation

$$\mathbf{F}_{st}(\mathbf{u}_0, \dot{\phi}, \beta) = \mathbf{f} \quad (5)$$

where $\mathbf{F}_{st}(\mathbf{u}_0, \dot{\phi}, \beta)$ holds the terms from the discretization of the structural equations, $\mathbf{u}_0 = [u_1, v_1, \theta_1, \dots, u_N, v_N, \theta_N]^T$ holds the elastic deformation at the N discretization points and \mathbf{f} holds the right hand side of (1) with the forces given by the aerodynamic forces (4) computed at each discretization point with aerodynamic coefficients from airfoil data.

3. Solution Scheme

The system of $3N$ nonlinear equations are solved using the following iterative scheme: 1) Choose operational condition: U_n and $\dot{\phi}$ and initial blade deflections \mathbf{u}_0 2) Compute apparent wind velocity and angle of attack using (2) and (3), respectively. 3) Compute the aerodynamic forces using (4), with (C_L, C_D, C_M) from the airfoil data. 4) Solve (5) for the new deflections \mathbf{u} . 5) If not converged return to 2. This gives the steady state deflections $\mathbf{u}_0 = \mathbf{u}_0(U_n, \dot{\phi})$. In the next section this method is used to compute the steady state blade deflection of the RWT blade for a speed up situation.

D. Linear Unsteady Aeroelastic Model

The nonlinear partial differential equation of motion (1) are linearized about the deflected blade position \mathbf{u}_0 and combined with the linearized unsteady aerodynamic model by Hansen et al.⁵ through linearized version of the apparent wind speed (2), angle of attack (3) etc.. The linear partial differential equation is:

$$\tilde{\mathbf{A}}\dot{\tilde{\mathbf{u}}} + \left(\tilde{\mathbf{A}}_{ss}\tilde{\mathbf{u}}''\right)'' + \left(\tilde{\mathbf{B}}_s\tilde{\mathbf{u}}'\right)' + \tilde{\mathbf{B}}\tilde{\mathbf{u}} = \tilde{\mathbf{F}}\tilde{\mathbf{f}} \quad (6)$$

where $\tilde{\mathbf{u}} = \tilde{\mathbf{u}}(s, t) = [u_1(s, t), v_1(s, t), \theta_1(s, t), \dot{u}_1(s, t), \dot{v}_1(s, t), \dot{\theta}_1(s, t), z_{1,1}(s, t), z_{2,1}(s, t), z_{3,1}(s, t), z_{4,1}(s, t)]^T$ are the linearized states and $\tilde{\mathbf{A}} = \tilde{\mathbf{A}}(\mathbf{u}_0, \dot{\phi}_0, \beta_0, U_{n,0})$, $\tilde{\mathbf{B}}_{ss} = \tilde{\mathbf{B}}_{ss}(\mathbf{u}_0, \dot{\phi}_0, \beta_0)$, $\tilde{\mathbf{B}}_s = \tilde{\mathbf{B}}_s(\dot{\phi}_0, \beta_0)$, $\tilde{\mathbf{B}} = \tilde{\mathbf{B}}(\mathbf{u}_0, \dot{\phi}_0, \beta_0, U_{n,0})$ are collections of the linear coefficients. All matrices are shown in Kallesøe.³ When linearized about the deflected blade the main effect from the geometric nonlinearities are preserved since terms like uv , which are zero when linearized about the undeflected blade, becomes $u_1v_0 + u_0v_1$ when linearized about the deflected blade. The 0 subscript denote the steady state part and the 1 subscript denotes the linear part. The spatial dependencies in (6) are approximated by the second order finite difference scheme, which leads to an ordinary differential equation of aeroelastic motion:

$$\mathbf{A}\dot{\mathbf{u}} + \mathbf{B}\mathbf{u} = \mathbf{0} \quad (7)$$

where $\mathbf{A} = \mathbf{A}(\mathbf{u}_0, U_{n,0}, \dot{\phi}_0, \beta_0)$ and $\mathbf{B} = \mathbf{B}(\mathbf{u}_0, U_{n,0}, \dot{\phi}_0, \beta_0)$ hold the coefficients from the finite difference approximation of (6) and \mathbf{u} holds the linear elastic deformations, velocities and aerodynamic states at each discretization point. Together with clamped-free boundary conditions (at the blade root and tip, respectively) the ordinary differential equation (7) forms a differential eigenvalue problem. The eigenvalues and corresponding eigenvectors can be grouped in two sets: Real valued eigenvalues and complex valued eigenvectors. The real valued eigenvalues are related to the aerodynamic states, and corresponds to time lags of the aerodynamic. The complex valued eigenvalues are related to the structural states and gives the

frequencies and damping of the aeroelastic modes of motion. It is noted that since aerodynamic forces are included the eigenvalue problem (7) is not self-adjoint and therefore the eigenvectors are not orthogonal. In next section, this model is used to compute two sets of damping, frequency and shapes of aeroelastic modes of motion of the RWT blade for a speed up situation, one including steady state blade deflection and one neglecting them.

III. Stability of the RWT blade

The effect of blade deflection on the aeroelastic stability is illustrated by comparing the aeroelastic modes of blade motion with and without blade deflection. The aeroelastic modes are computed for zero pitch angle, a wind speed on 10 m/s and a series of rotor speeds. The nonlinear steady state aeroelastic model (5) is used to compute steady state blade deflections under the assumption of constant inflow (no shear or tower effects) and no gravity. The linear unsteady aeroelastic model (7) is used to compute the aeroelastic frequencies, damping and mode shapes for the deflected blade and the undeflected blade. Furthermore the same series of rotor speeds are also simulated with nonlinear aeroelastic code HAWC2^{6,7} for zero pitch angle and 10 m/s wind. The damping of the least damped mode is then estimated by the exponential decay/growth of the initial blade oscillation.

A. Steady State Blade Deflections

The method described in the previously section is used to computer the steady state elastic blade deflections of the RWT blade for different rotational speeds. Figure 1 shows the edgewise, flapwise blade tip deflection and the angle of attach (AOA). The angle of attach is included to compare the blade twist of the two models. The results from the present model are compared with results from HAWC2 simulations. The

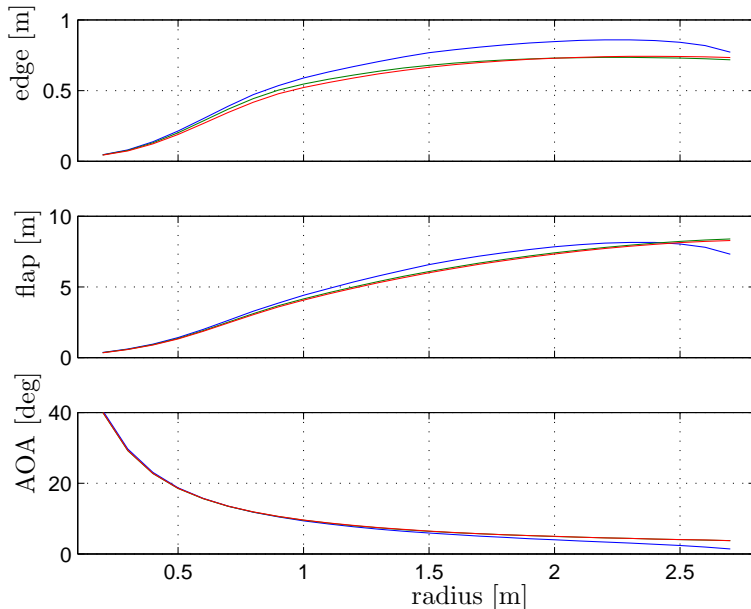


Figure 1. Steady state tip deflection and angle of attack at 90 % radius at a free wind on 10 m/s and varying rotational speed. Blue line: HAWC2, green line: FD with 80 nodes, and red line: FD with 90 nodes.

HAWC2 simulations are performed with an very high structural damping to suppress any unstable dynamic effects. The results from the present model are shown for $N = 80$ and $N = 90$ discretization points. The two results are seen to be on top of each other, indicating that the solution is converged at $N = 80$, and this number of discretization point is used in the rest of this work. There is a reasonable good agreement between the results from the present model and HAWC2 for most rotor speeds. At high rotor speeds the difference become considerably, this is because the HAWC2 solution twist more than the present model, reducing the angle of attach and thereby the aerodynamic forces. The second order formulation of the present model is

only valid for a reasonable deflection, where the multi-body formulation of HAWC2 is valid for arbitrary large deflections. So, the difference at the largest blade deflections is assumed to be caused by the different formulations.

B. Aeroelastic Stability

The damping, frequencies and shapes of aeroelastic modes of motion for the RWT blade are computed for both a steady state deflected blade and an undeflected blade. Figure 2 shows the aeroelastic frequency for the first five blade modes under the different operation conditions for the undeflected and deflected blade, and the dominant frequency of the transient response in the HAWC2 simulations. Figure 3 shows the corresponding

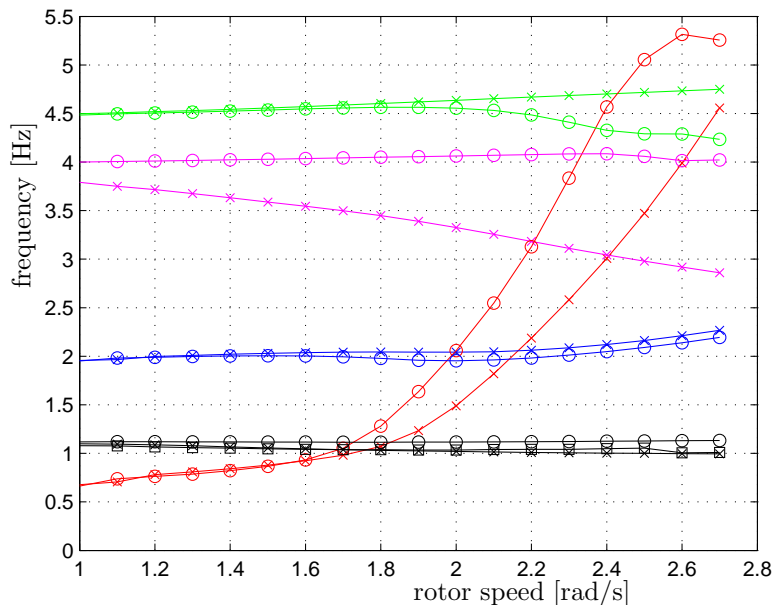


Figure 2. Aeroelastic frequencies of first flapwise (red), first edgewise (black), second flapwise (blue), second edgewise (magenta) and third flapwise (green) modes versus rotor speed. The circles (o) denotes frequencies for the undeflected blade and crosses (x) denotes frequencies for the deflected blade. The black boxes (\square) denote the dominant frequency of the transient response of in the nonlinear simulation with HAWC2.

aeroelastic damping, except for the first and second flapwise bending modes which are highly damped and therefore not shown.

The first edgewise bending mode (the second mode) become negative damped for rotor speeds above 1.9 rad/s for the deflected blade, while it stays positive damped for the undeflected blade. The HAWC2 simulations agree well with the result from the deflected blade. Figure 4 shows the cross section motion at 75% radius for the first edgewise mode for three different rotations speeds. The direction of vibration are seen to shift sign for the deflected blade. The coupling of the edgewise bending with blade torsion creates an aerodynamic coupling between edgewise and flapwise bending through the lift-torsion coupling. The direction of vibration is related to the aerodynamic damping, and it is assumed that the negative aeroelastic damping of the first edgewise bending mode for the deflected blade is caused by this phase shift. The second edgewise bending mode (fourth mode) and the third flapwise bending mode (the fifth mode) become flutter modes around 2.6 rad/s for the undeflected blade. For the deflected blade it is only the second edgewise mode which becomes a flutter mode. The jumps in damping around 2.6 rad/s for the HWAC2 simulations are caused by the negative damped flutter mode at theses rotation speeds. Figure 5 shows that the fourth mode of the undeflected blade changes direction of vibration from counter clockwise to clockwise at 2.6 rad/s, and that this causes the mode to become negative damped. The deflected blade, vibrates in clockwise direction for all the shown rotor speeds, indicating that this is the reason for the deflected blade to become negative damped at a lower rotor speed than the undeflected blade. The third flapwise mode (fifth mode) for the deflected blade stays positive damped for all the shown rotor speeds while the undeflected blade become

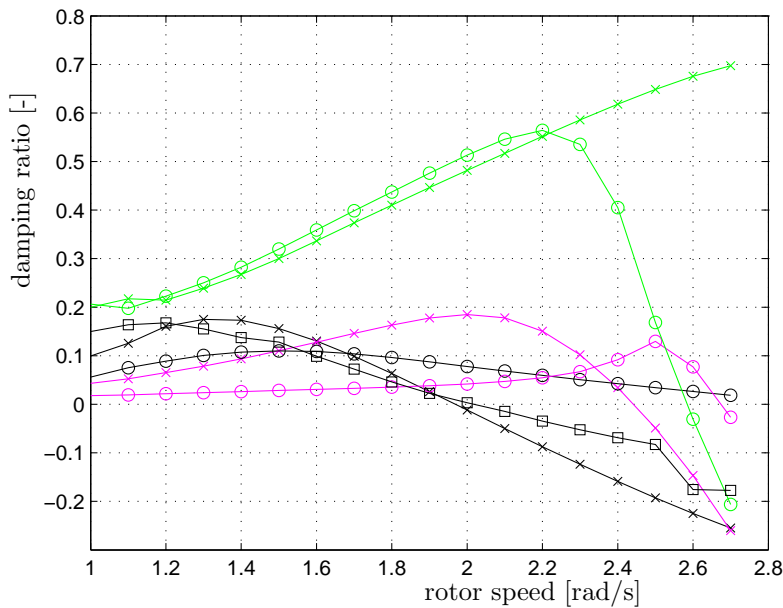


Figure 3. Aeroelastic damping of first edgewise (black), third flapwise (green), and second edgewise (magenta) modes versus rotor speed. The circles (o) denote damping for the undeflected blade, and the crosses (x) denote results for the deflected blade. The black boxes (\square) denote the damping of the transient response in the nonlinear aeroelastic simulation with HAWC2.

negative damped for rotor speeds above 2.5 rad/s. The reason for this difference between the deflected and undeflected blade is caused by the frequencies for the second edgewise mode and the third flapwise mode become close for the undeflected blade, giving an interaction between the two modes.

It is noted that the rated rotor speed for this turbine is 1.26 rad/s. So, all the instabilities occur well above rated rotor speed.

IV. Conclusion

The effects of steady state deflections of a wind turbine blade on its stability limits, especially with regards to the flutter limit, are analyzed. The coupling of edgewise bending and torsion due to flapwise blade bending are assumed to have some effects on the flutter limits of wind turbines.¹ In the present work, the aeroelastic blade model suggested by Kallesøe^{2,3} is used to investigate the aeroelastic stability limits of the RWT blade with and without the effects of the steady state blade deflection. The investigation shows a slightly decreased flutter limit on the rotor speed due to the blade deflection, and that the first edgewise bending mode becomes negatively damped due to the coupling with blade torsion which causes a change of the effective direction of blade vibration. These observations are confirmed by nonlinear aeroelastic simulations using the HAWC2^{6,7} code.

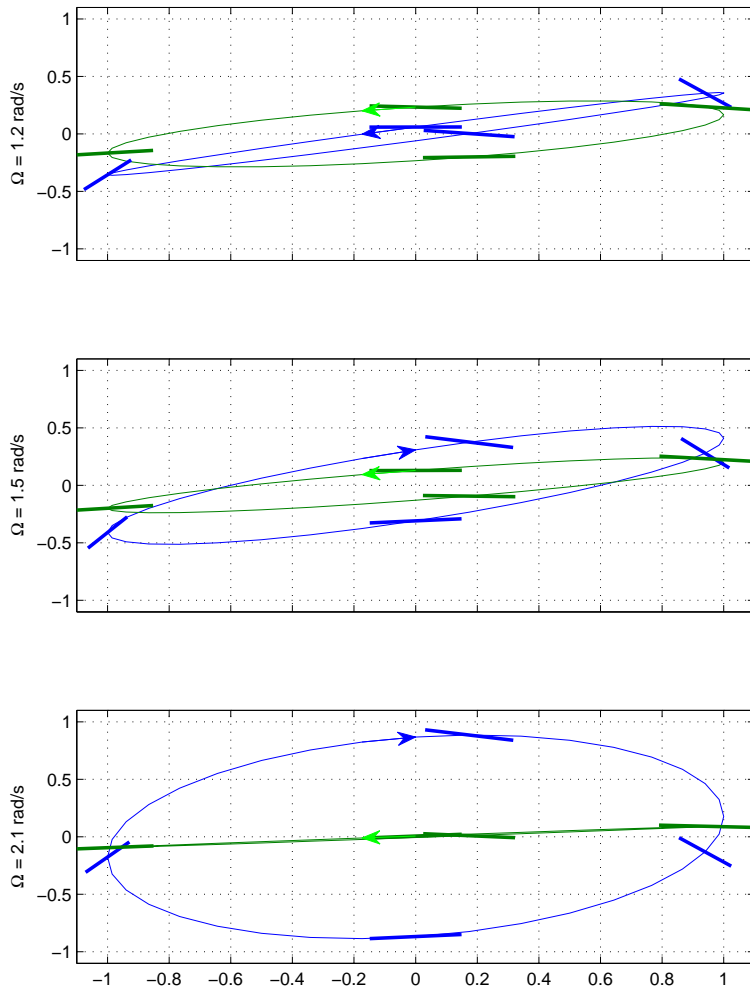


Figure 4. Traces of cross-sectional blade motion at 75 % radius in the first edgewise bending mode at different rotor speeds for the undeflected (green traces) and deflected (blue traces) blade with exaggeration of the torsional component with a factor of 1000. Arrows denote the direction of motion. Top, middle and bottom figures show the results for the rotor speeds 1.2, 1.5 and 2.1 rad/s, respectively. Note that the relative wind comes from right to left in the displayed cross-sectional coordinate system.

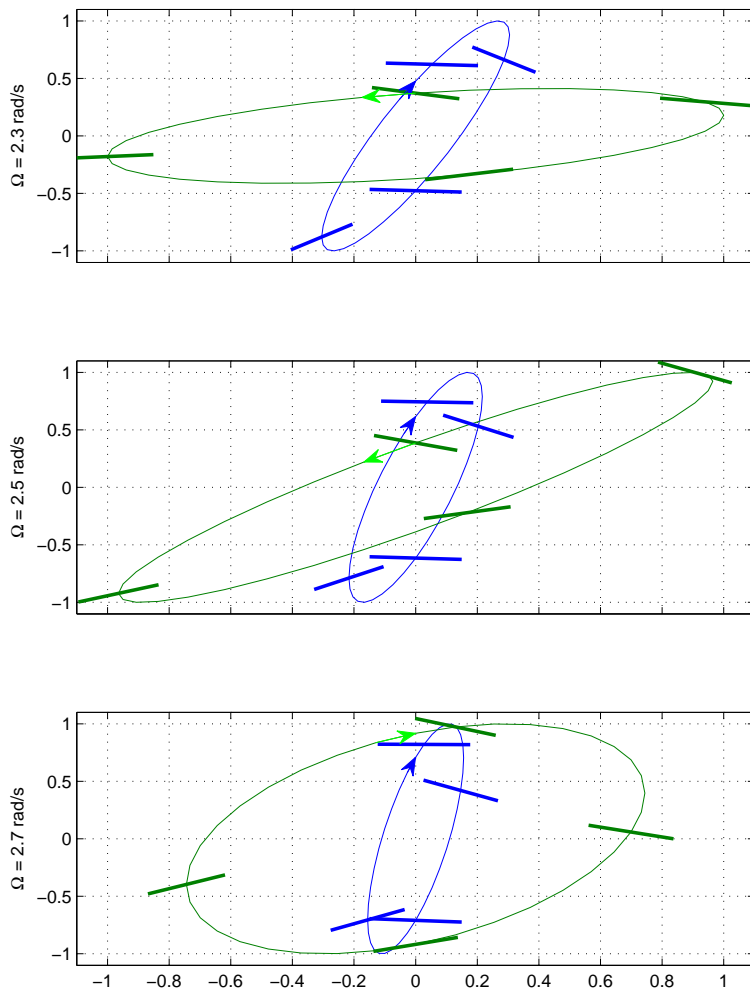


Figure 5. Traces of cross-sectional blade motion at 90 % radius in the second edgewise bending mode at different rotor speeds for the undeflected (green traces) and deflected (blue traces) blade with exaggeration of the torsional component with a factor of 300. Arrows denote the direction of motion. Top, middle and bottom figures show the results for the rotor speeds 2.3, 2.5 and 2.7 rad/s, respectively. Note that the relative wind comes from right to left in the displayed cross-sectional coordinate system.

References

- ¹Hansen, M., "Aeroelastic instability problems for wind turbines," *Wind Energy*, Vol. 10, No. 6, 2007, pp. 551–577.
- ²Kaltesoe, B., "Equations of motion for a rotor blade, including gravity, pitch action and rotor speed variations," *Wind Energy*, Vol. 10, No. 3, 2007, pp. 209–230.
- ³Kaltesøe, B., *Aeroservoelasticity of Wind Turbines*, PhD thesis, Technical University of Denmark, Department of Mechanical Engineering, April 2007.
- ⁴Jonkman, J., "NREL 5 MW Baseline Wind Turbine," Tech. rep., NREL/NWTC, 1617 Cole Boulevard; Golden, CO 80401-3393, USA, 2005.
- ⁵Hansen, M., Gaunaa, M., and Madsen, H., "A Beddoes-Leishman type dynamic stall model in state-space and indicial formulation," Tech. Rep. Risø -R-1354(EN), Risø National Laboratory, (available from www.risoe.dk), August 2004.
- ⁶Larsen, T., Hansen, A., and Buhl, T., "Aeroelastic effects of large blade deflections for wind turbines," *Proceedings of the special topic conference "The Science of making Torque from Wind"*, 2004, pp. 238–246.
- ⁷Larsen, T., Madsen, H., Hansen, A., and Thomsen, K., "Investigations of stability effects of an offshore wind turbine using the new aeroelastic code HAWC2," *Proceedings of the conference "Copenhagen Offshore Wind 2005"*, 2005.
- ⁸Hansen, M. O. L., *Aerodynamics of Wind Turbines*, James & James, 2001.
- ⁹Kaltesøe, B., "A low-order model for analysing effects of blade fatigue load control," *Wind Energy*, Vol. 9, No. 5, 2006, pp. 421–436.